# Improvement of zero valent iron nanoparticles by ultrasound-assisted synthesis, study of Cr(VI) removal and application for the treatment of metal surface processing wastewater

Nourhane Bounab, Laurent Duclaux, Laurence Reinert, Abdelkrim Oumedjbeur, Chahrazed Boukhalfa, Philippe Penhoud, Fabrice Muller

# Improvement of zero valent iron nanoparticles by ultrasound-assisted synthesis, study of Cr(VI) removal and application for the treatment of metal surface processing wastewater

Nourhane Bounab (Validation) (Formal analysis) (Investigation) (Writing - original draft) (Writing - review and editing) (Visualization) (Project administration), Laurent Duclaux (Methodology) (Validation) (Investigation) (Writing - original draft) (Writing - review and editing) (Visualization) (Supervision) (Project administration) (Funding acquisition), Laurence Reinert (Methodology) (Validation) (Investigation) (Writing - original draft) (Writing - review and editing) (Visualization) (Supervision) (Project administration) (Funding acquisition), Abdelkrim Oumedjbeur (Validation) (Writing - review and editing) (Visualization) (Funding acquisition), Chahrazed Boukhalfa (Validation) (Visualization) (Supervision) (Project administration) (Funding acquisition), Philippe Penhoud (Formal analysis) (Investigation), Fabrice Muller (Validation) (Investigation) (Visualization)

PII: S2213-3437(20)31122-2

DOI: https://doi.org/10.1016/j.jece.2020.104773

Reference: JECE 104773

To appear in: *Journal of Environmental Chemical Engineering*

Received Date: 3 October 2020

Revised Date: 10 November 2020

Accepted Date: 16 November 2020

Please cite this article as: Bounab N, Duclaux L, Reinert L, Oumedjbeur A, Boukhalfa C, Penhoud P, Muller F, Improvement of zero valent iron nanoparticles by ultrasound-assisted synthesis, study of Cr(VI) removal and application for the treatment of metal surface

processing wastewater, *Journal of Environmental Chemical Engineering* (2020),
doi: https://doi.org/10.1016/j.jece.2020.104773

# Improvement of zero valent iron nanoparticles by ultrasound-assisted synthesis, study of Cr(VI) removal and application for the treatment of metal surface processing wastewater

Nourhane Bounab[a,b], Laurent Duclaux[a*], Laurence Reinert[a], Abdelkrim Oumedjbeur[a], Chahrazed Boukhalfa[b], Philippe Penhoud[c], Fabrice Muller[c]

[a] *Université Savoie Mont Blanc, LCME, F73000, Chambéry, France*

[b] *Laboratory of Pollution and Water Treatment, Chemistry Department, Université Frères Mentouri Constantine 1, Constantine, Algeria*

[c] *Institut des Sciences de la Terre d'Orléans (ISTO), CNRS-Université d'Orléans, 1A Rue de la Férollerie CS 20066, F45071, Cedex 2, Orléans, France*

*corresponding author : Laurent Duclaux
Laurent.duclaux@univ-smb.fr



## Graphical Astract

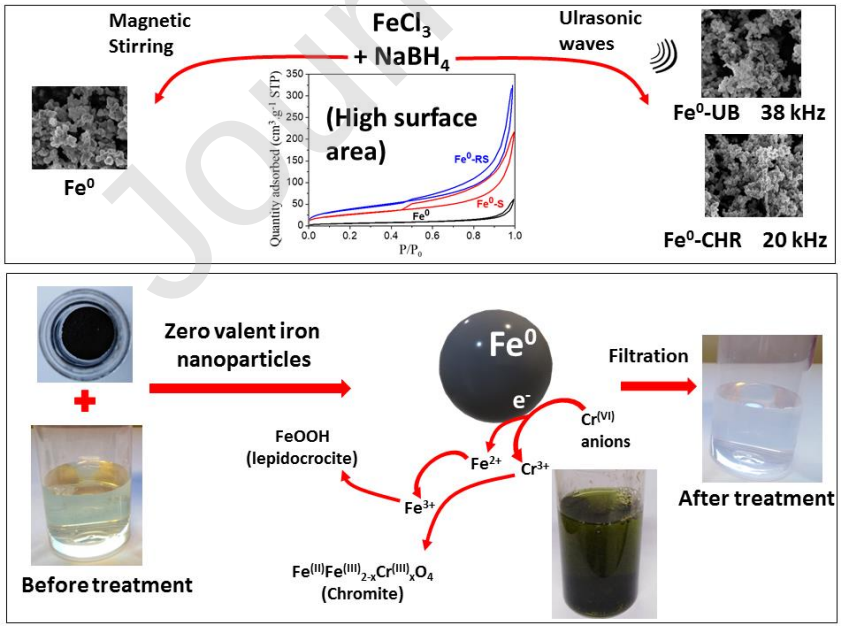

## Highlights

- Zero valent iron nanoparticles prepared for the removal of Cr(VI)
- Ultrasound-assisted synthesis at 20 kHz yields to highest surface area
- Faster Cr(VI) reduction of sonicated nanoparticles than ones prepared by stirring
- Co-precipitation of Cr(III) and Fe ions in the form of chromite
- Efficient industrial wastewater treatment by ultrasound-prepared Fe nanoparticles

## Abstract

Reductive zero-valent iron nanoparticles were prepared for the treatment of Cr(VI) solutions. The ferric ions reduction by borohydride was carried out through mechanical stirring or ultrasound irradiation either in an ultrasonic bath or in a 20 kHz cup-horn reactor.

The prepared materials have been characterized by X-ray diffraction, infrared spectroscopy, scanning electron microscopy, and $N_2$ adsorption-desorption at 77 K. The microscopic observations showed iron nanoparticles with diameter in the range 40 nm-80 nm, arranged in chain aggregates regardless the variation of the preparation method. The ultrasonic synthesis allowed to obtain higher BET specific surface area (99 $m^2.g^{-1}$ for nanoparticles prepared in ultrasonic bath and 145 $m^2.g^{-1}$ for the ones prepared by probe sonication) than the ones of samples synthesized in silent conditions (22 $m^2.g^{-1}$).

The Cr(VI) ions removal in pure water solution was found significant at acidic pH. The removal kinetics modeled by pseudo first order, are linearly proportional to the BET surface areas. They are rapid (< 30 min to attain equilibrium), and decrease as increasing the Cr(VI) concentration and as decreasing the iron nanoparticles dose. Cr(VI) ions were removed by reduction and co-precipitation of Cr(III) in the form of chromite at pH>7. The iron nanoparticles were tested for the treatment of metal surface processing wastewater. For such treatment, they have proven to be efficient for removing Cr(VI) together with Ni(II) ions. The iron nanoparticles prepared by 20 kHz ultrasonic probe have been found more effective for Cr(VI) removal than any kind of iron nanoparticles conventionally prepared.

**Keywords:** iron nanoparticles, ultrasound, Cr(VI), industrial effluent, chemical reduction, kinetics

## 1. Introduction

Zero-Valent Iron (ZVI or Fe(0)) is the most commonly used zero-valent metal for environmental remediation [1]. Since the early 1990s, this reducing agent has been used to remediate a wide variety of organic and inorganic contaminants present in various environmental media (ground and surface waters, soils) [2-3]. Among the most common species treated by ZVI are many anions such as nitrates, bromates, chlorates [4], chlorinated organic compounds [5], dyes [6], heavy metals and metalloids [7-8], among them, hexavalent chromium [9-12]. Hexavalent chromium species are well known as human carcinogens. Their occurrence in groundwater and soils mainly results from industrial activities (e.g., stainless steel or pigment production, metal plating, leather tanning, etc.) that largely contribute to their dispersion in the environment, thus causing serious human health hazards and ecological issues [13]. The World Health Organization (WHO) has recommended a limit concentration of total Cr(VI) in drinking water of 0.05 $mg.L^{-1}$. This limit is supposed to insure an adequate protection level of health [14]. Even if in most of the developed countries, the average occurrence levels of total Cr in drinking-water are arround 1 $\mu g.L^{-1}$, in some developing countries, local values often exceed the recommended ones. In European Union countries, limits for chromium emissions in the aquatic environment depend on the source of contamination and its speciation (Cr(VI), Cr(III)) [15]. In France, the liquid waste discharge into the natural environment is limited to 50 $\mu g.L^{-1}$ for Cr(VI) and 100 $\mu g.L^{-1}$ for $Cr_{total}$, if the discharge exceeds 1 g/day and 5 g/day respectively, [16]. In Algeria, chromium discharges in industrial water are limited to 100 $\mu g.L^{-1}$ and 2000 $\mu g.L^{-1}$ for Cr(VI) and Cr(III), respectively [17]. Many methods have been studied to remove Cr(VI) from water, in particular anionic exchange using functionalized organic resins [18-19], reverse osmosis [20], adsorption onto various materials [21], as well as the reduction into Cr(III) and further precipitation [22]. Although many different metallic species (Al, Cu, Mg, Si, Zn and Cu; etc.) have been studied for the reduction of Cr(VI) into Cr(III), iron remains one of the most frequently used metal. Indeed, its use is widely cited in the literature. By contrast metals possessing high reductive properties show inactivating effects due to their rapid corrosion [23].

Lots of studies have reported the use of mixed systems in which the ZVI particles are

combined with other materials, either to improve the treatment efficiency of Cr(VI) or to prevent its release in the environment, favored by a powdered form. Among the materials used to support ZVI particles are organic resins [24], various carbon materials such as activated carbon fibers [25], carbon nanotubes [26], biochar [27-28], and different clays such as sepiolite [29], bentonite [30-31] or vermiculite [32]. Nevertheless, the presence of these supports induces a decrease of both mass transfer and ZVI reaction rate. For these main reasons, researches have also focused on the reductive properties of non-supported ZVI.

Pure ZVI has been applied in different shapes for the depollution of aqueous media: in the form of fibrous steel wool [33], wires, cylinders, spheres or particles of milli-, micro- or nanometric sizes [34]. The reduction efficiencies of ZVI have been evaluated through the effects of diverse parameters such as particles' shape and size, and also experimental conditions (such as pH, temperature, Cr(VI) initial concentration, ZVI introduced dose, matrix nature, etc.).

Cissoko et al. [35] have studied the Cr(VI) removal from simulated contaminated ground-water using either metal filings, and ZVI micron or nanoscale powders. They have shown that the Cr(VI) reduction was favored by high $Fe^0$ dosage and temperature as well as low pH values and Cr(VI) concentrations. Using a micrometric powder, in optimal conditions (pH 5.5, pollutant concentration of 20 $mg.L^{-1}$ and $Fe^0$ dose of 10 $g.L^{-1}$) the total amount of Cr(VI) was removed after 2 hours reaction time. The efficiency comparison has indicated that nanoscale ZVI had a significant high reductive efficiency, but powder and metal filings kept longer activity. The reaction kinetics obtained by these authors [35] could be described as a pseudo-first-order model. In another study, Fiúza et al. [36] have shown that the kinetic rate of Cr(VI) reduction depended strongly on the surface characteristics of the iron particles such as their superficial oxidation state and available surface area. These authors have simulated the kinetic of the Cr(VI) reduction heterogeneous reaction by a shrinking particle type model instead of using a pseudo-first-order kinetics. They demonstrated that the kinetic rate was proportional to the available iron surface area, to the solution initial volume and to the Cr(VI) concentration.

Some other references mentioned the particle size of ZVI as a key parameter for the Cr(VI) reduction. Indeed, nanometric sizes (labeled nZVI) were very efficient and exhibited an enhanced reactivity in comparison with other ZVI materials. As for

example, Montesinos et al. [37] have obtained a complete conversion of an initial 0.3 mmol.$L^{-1}$ Cr(VI) concentration (pH 3) after only 30 min with a nZVI/Cr(VI) molar ratio of 3. However, the reduction of Cr(VI) by nZVI has yielded to the Fe(III)/Cr(III) oxides/oxyhydroxides layer formation on the outer surface of the nZVI particles, thus limiting their efficiency. Different methods have been developed to obtain nanosized iron particles. Very recently, Zhang et al. [38] have obtained chitosan loaded nanoscaled-ZVI materials by reduction of a chitosan/Fe(II) solution with $NaBH_4$. Green synthesis of ZVI using leaf-extracts of various plants constitutes a very recent eco-friendly alternative to chemically synthesized ZVI. By mixing Fe(III) solutions with previously purified leaf-extracts possessing high antioxidant properties, iron nanoparticles of sizes ranging between ~40 and 50 nm could be prepared [39-40]. Furthermore, the use of ultrasounds for iron particles' preparation constitutes one of the most interesting routes. In fact the ultrasounds increase the number of active surface sites by increasing both the external surface and the specific surface area of the iron particles [41]. Some iron particles of nanometric size were obtained by Jamei et al. [42] by reduction under ultrasounds (using a 20 kHz probe) of an aqueous Fe(II) solution with $NaBH_4$. The authors have shown that the nanoparticles morphology changed from spherical to plate and needle type, depending on applied the ultrasonic power. Nanoparticles of sizes ranging between ~ 30 to 90 nm and BET surface areas between 10 to 42 $m^2.g^{-1}$ have been obtained. Zhou et al. [43] have tested some nZVI particles (of sizes in the 50-70 nm range) similarly prepared for the reduction of Cr(VI) through ultrasounds irradiation. They highlighted the contribution of ultrasound for the surface activation of nZVI particles by inducing many new reactive sites and thus promoting the Cr(VI) chemical reduction. Moreover, the ultrasound could also remove the by-products covering the nZVI particles surface, thus increasing the reactive sites accessibility. The aim of this work was to compare the efficiency of nZVI particles prepared by conventional method or under ultrasound for the reduction of Cr(VI) in aqueous solution.

Both an ultrasonic bath (38 kHz) and a cup-horn reactor (20 kHz) were used for the ultrasound-assisted preparation. The obtained particles were fully characterized in terms of size, crystallinity, porosity and surface chemistry, using the classical methods of solids characterization, i.e., X-Ray Diffraction (XRD), Infrared spectroscopy (IR), $N_2$ adsorption-desorption measurements and Field Emission Gun

Scanning Electron Microscopy (FE-SEM). Their efficiencies for Cr(VI) reduction were studied both in water solutions and in a metal surface treatment wastewater and correlated to their structural and textural properties.

## 2. Material and methods

### *2.1. Preparation of zero-valent iron nanoparticles*

The iron nanoparticles were prepared firstly by using the conventional method described by Wang et al. [44]. Ferric ions have been reduced in water of Ultra High Quality (UHQ : 18 MΩ.cm). In a three-necked flask, a 0.4 mol.$L^{-1}$ sodium borohydride ($NaBH_4$, 98%, Acros, France) solution (100 mL) was added dropwise to a freshly prepared 0.1 mol.$L^{-1}$ solution (100 mL) of ferric ions ($FeCl_3.6H_2O$ 99,5%, Prolabo, France) mechanically stirred at 200 rpm for 30 min under nitrogen atmosphere. The iron solution was deoxygenated for 15 min by bubbling nitrogen gas prior to its mixture with $NaBH_4$ and maintained under nitrogen atmosphere during the synthesis. The iron (III) reduction leading to $Fe^0$ nanoparticles and to dihydrogen through the hydride oxidation can be described by the following equation (1):

$4\ Fe^{3+} + 3\ BH_4^- + 9\ H_2O = 6\ H_2 + 4\ Fe^0 + 3\ B(OH)_3 + 9\ H^+$ .....(1)

According to this reaction, acidity is produced during the reduction. However, the measured final pH after the synthesis of iron nanoparticles was about 8. This pH value can be explained by the hydrolysis of the excess borohydride which can be catalyzed (acidic catalysis) by the produced protons (reaction 2):

$BH_4^- + H^+ + 3\ H_2O = B(OH)_3 + 4\ H_2$ .....(2)

The acido- basicity of the solution depends on reaction (3):

$B(OH)_3 + H_2O = B(OH)_4^- + H^+$ .....(3)

As sodium borohydride is in excess with respect to iron (III) cations, its hydrolysis [45] can also occur through reactions (4) and (5),

$3\ BH_4^- + 2\ H_2O = BO_2^- + 4\ H_2$ .....(4)

$BH_4^- + 4\ H_2O = B(OH)_4^- + 4\ H_2$ .....(5)

A more realistic reaction the iron (III) reduction leading to $Fe^0$ nanoparticles is given by reaction (6) which takes into account both redox equation (1) and the acid-catalysed hydrolysis of borotetrahydride (equation 2) leading possibly to a final pH close to 8, as observed experimentally:

$Fe^{3+} + 3\ BH_4^- + 9\ H_2O = Fe^0 + 3\ B(OH)_3 + \frac{21}{2} H_2$ .....(6)

The final pH of the solution after the iron nanoparticle synthesis was measured at 8 close the pKa value (pKa of the $B(OH)_3/B(OH)_4^-$ couple is equal to 9.28) which means that on one hand $B(OH)_3$ is formed through reaction (6) and on the other hand $B(OH)_4^-$ is produced through hydrolysis of excess of $BH_4^-$ (reaction 5).

Under ultrasonic conditions, iron nanoparticles were prepared in the same conditions as previously described in two manners. In the first one, the three-necked flask was sonicated for 30 min in an ultrasonic tank (Eumax, UD80SH-1.3L, 38 kHz, China) (Figure S1 (a)). The temperature was maintained at 25°C by tap water circulation in a copper cooling coil placed in the bath. In the second, the preparation was carried out in a 1.5 L cup-horn jacketed reactor (Figure S1 (b)) (Synetude, Cognin, France, 20 kHz, 47 mm probe diameter, amplitude set to 75%) for 30 min, using both 250 mL of $FeCl_3.6H_2O$ solution and $NaBH_4$ reducing solution added dropwise. The temperature in this reactor was maintained constant at 25°C by circulation of tap water in the double jacket. Prior to sonication, the iron solution was deoxygenated with nitrogen gas for 15 min in order to avoid the presence of dissolved carbon dioxide and dioxygen gases. The sonication was performed through bubbling of nitrogen gas.

The volumic acoustic power, determined by calorimetric measurement [46], was 12 W/L for the 38 kHz ultrasonic bath and 80 W/L for the 20 kHz cup-horn reactor. The dissipated power by mechanical agitation used for the synthesis in silent condition is less than 0.01 W/L owing to viscosity of the fluid.

The real electric powers consumed by the ultrasonic devices were measured at 60 W and 160 W for the ultrasonic bath (38 kHz) and the cup-horn reactor (20 kHz), respectively. For comparison, in the silent condition; the electrical energy consumption was about 3 W for the orbital agitation of a flask (at 200 rpm).

All the prepared solids were collected and vacuum filtrated by membrane filters, (0.45 µm pore size, Durapore®), under nitrogen flow. The collected powder was washed four times with a total volume of 150 mL of pure ethanol, and then vacuum-dried at $10^{-2}$ mbar using a primary pump equipped with a liquid nitrogen trap. Finally, the ZVI nanoparticles were stored under argon atmosphere in a desiccator before any use. The ZVI nanoparticles prepared in silent conditions are referred to $Fe^0$ while the ones synthesized in the ultrasonic bath and in the cup-horn reactor are referred to $Fe^0$-UB and $Fe^0$-CHR, respectively.

*2.2. Solid characterization*

The prepared nanoparticles were characterized by X-Ray Diffraction (XRD) in the transmission mode (Debye-Scherrer geometry) using a diffractometer (λCoKα1 = 0.1789 nm) equipped with a INEL CPS120 detector (INEL, Artenay , France) with a resolution of 0.03° calibrated with NAC ($NaCa_2Al_3F_{14}$), and an INEL generator (35 kV, 35 mA). Typical X-ray diffractogramms were obtained after irradiation of 7.5 h on rotating glass capillaries (0.3 mm diameter, glass 050 Hilgenberg Gmbh) filled with the milled ZVI nanoparticles. The residual solids recovered after treatment of the Cr(VI) solutions made from UHQ water, were also characterized by XRD using the same diffractometer calibrated with $Y_2O_3$. Typical diffractograms in the reflexion mode were obtained after irradiation of 1 h of the solids deposited on an aluminium plate sample holder at a 5° incident angle.

Infrared spectroscopy analyses of the ZVI nanoparticles were performed by using a Thermo Scientific Nicolet IS10 infra-red spectrometer (ThermoElectron SAS, France) on pellets obtained by compaction under a pressure of 440 MPa using an hydraulic pump. These pellets were made of a mixture of 0.1 mg iron nanoparticles and of ~400 mg of dried KBr (IR grade, >99.5%, Chimie-Plus) and then stored in a desiccator before analysis. A KBr pellet was used as a reference. All spectra were collected from 400 to 4000 $cm^{-1}$ with a 4 $cm^{-1}$ spectral resolution. Each acquisition was performed on 64 scans.

An automatic sorptometer (ASAP 2020, Micromeritics, USA) was used to determine the specific surface area, the porosity, and the pore size distribution by adsorption–desorption of $N_2$ at 77 K. The samples of ZVI nanoparticles were degased under a vacuum (2 μmHg) at 25°C for more than 48 h prior to analysis. The specific surface area of the ZVI nanoparticles was calculated by the Brunauer–Emmett–Teller (BET) equation in the 0.05 to 0.35 relative pressure range. In addition, the pore size distributions were calculated by the Barrett-Joyner-Halenda desorption model (BJH) on the desorption branch of the isotherm.

The various samples were observed by scanning electron microscopy using a ZEISS ULTRA 55 Gemini Field Emission Gun Scanning Electron Microscope (FEG-SEM, Zeiss, Germany) coupled to an energy-dispersive spectrometer (EDS) equipped with a

Silicon Drift Detector (BRUKER AXS- 30 $mm^2$, Germany).

### *2.3. Experimental of Cr(VI)/metal removal studies*

All chemicals reagents used in this study were of analytical grade. Cr(VI) removal was studied on one hand in UHQ water and on the other hand in an industrial wastewater.

The removal of Cr(VI) ions by the prepared nanoparticles was studied in batch as a function of pH and contact time. Cr(VI) standard solutions were prepared from $K_2CrO_4$ (99.5%, Prolabo, France) dissolution in deionised UHQ water (18 MΩ.cm). For the pH effect study of the Cr(VI) removal, 100 mL of Cr(VI) solutions were prepared at 10 $mg.L^{-1}$ in closed glass 250 mL flasks and their pH was adjusted in the range [2-8] by using HCl or NaOH solutions prior to the ZVI nanoparticles addition. Thus, the solutions were agitated for 1 h in a temperature-regulated orbital shaker (170 rpm) in the presence of the ZVI nanoparticles at 22°C. The pH was measured using a 3510 pH meter (Jenway). The concentration of Cr(VI) ions were determined after filtration on membrane filters (MF-Millipore™ 0.45 µm pore size). The Cr(VI) removal kinetics were studied at 22°C and at pH 2 in 1 L of Cr(VI) solution at 10 $mg.L^{-1}$ (or 20 $mg.L^{-1}$), under mechanical stirring in an orbital shaker (170 rpm). Typically, a weighted amount of ZVI nanoparticles: 10 mg (or 1 mg) was added into an agitated Cr(VI) solution of a given pH. Furthermore, at some selected times in the range [0.5-60 min], 10 mL was collected from the reaction solution for further analysis by a syringe equipped with Membrane Filter (MF-Millipore™, 0.45 µm pore size).

The concentrations of Cr(VI) ions were analysed by using a UV-Visible spectrophotometer (Varian, Cary 50 Scan), after complexation with 1.5-diphenylcarbazide ($C(NH)_4O(C_6H_5)_2$) (4 %) prepared in ethanol and in the presence of concentrated sulfuric acid (10 %). For each Cr(VI) analysis assay, a volume of 10 mL of Cr(VI) solution was mixed with 0.6 mL of diphenylcarbazide solution. In this method, Cr(VI) is reduced to Cr(III) by the 1,5-diphenylcarbazide which oxidizes to diphenylcarbazone ($C(NH)_2N_2O(C_6H_5)_2$). A coloured complex is formed of which absorbance is measured at 540 nm. The detection limit given is about 5 $\mu g.L^{-1}$ with a 5% accuracy [47]. For calibration, a series of Cr(VI) solutions was prepared in the

range of 0.25 mg.L$^{-1}$ to 2.5 mg.L$^{-1}$. Efficiency of Cr(VI) removal was calculated by using the following equation (7):

$$Cr(VI)\ removal\ efficiency\ (\%) = \left(\frac{C_0 - C_f}{C_0}\right) \times 100 \quad \text{.....(7)}$$

where $C_0$ and $C_f$ are respectively the initial and the residual concentrations (mg.L$^{-1}$). Cr(VI) removal experiments were also carried out on wastewater from surface treatment industry provided by a hazardous waste collecting company (Dechamboux Déchets Services "La Roche-sur-Foron", France). The removal efficiencies of Cr(VI) ions and other metallic ions (mainly Ni(II)) were studied for the three prepared ZVI nanoparticles types and compared to their efficiencies in the UHQ water solutions. Metals contents were determined by Inductively Coupled Plasma-Atomic Emission Spectroscopy (ICP-AES 720ES, Agilent, USA) at Geochemistry-Mineralogy ISTerre platform (University Grenoble Alpes, France). The ICP calibration solutions were prepared by using multi-element solutions (Al, Ag, As, B, Be, Bi, Ca, Cd, Co, Cr, Cu, Fe, K, Li, Mg, Mn, Mo, Na, Ni, Pb, Sb, Se, Sr, Ti, Tl, V, Zn, from Roth France) at 100 mg.L$^{-1}$ diluted with 2% HNO3 to obtain concentrations in the range 0.05 mg.L$^{-1}$-10 mg.L$^{-1}$.

The Chemical Oxygen Demand (COD) of the industrial wastewater was determined by using the protocol of the NF T.90.101 French standard through an oxidation with a potassium dichromate ($K_2Cr_2O_7$) excess, in a strong acid medium (sulfuric acid), under heating (reflux at 150 °C for two hours) and in the presence of a silver salt catalyst and mercuric salts (complexing chloride ions). The $Cr_2O_7^{2-}$ excess was then determined by colorimetry.

Table 1, summarizes the wastewater composition characterized by an acidic pH and by the significant presences of organic matter, Ni(II) and Cr in the form of Cr(VI) anion and Cr(III) cation. This wastewater was diluted by a factor of about 100, in order to test the Cr(VI) removal of a diluted effluent (at 0.14 mg.L$^{-1}$ Cr(VI) concentration).

The ZVI nanoparticles of three types (weight 10 or 60 mg) were mixed with 100 mL of the industrial wastewater and its diluted version. Then the suspensions were stirred in an orbital shaker (170 rpm) at 22°C for 1 h. The analyses of the filtrated

solutions after treatment by the ZVI nanoparticles were performed by ICP-AES (Table 3).

## 3. Results and discussion

### *3.1. Characterization of zero-valent iron nanoparticles*

#### *3.1.1. X-ray diffraction*

The X-ray diffraction patterns (Fig. 1) display broaden peaks at $2\theta$ = 53.26° (*110* line); and $2\theta$ = 78.65° (*200* line) due to the presence of centered cubic α-Fe lattice. The very thin line at $2\theta$ = 36.9° in the $Fe^0$ diffractogramm is attributed to the presence of $NaBO_2$ impurities probably at the surface of the iron nanoparticles, deriving from the $NaBH_4$ reducer hydrolysis. These diffractogramms are quite different from the ones obtained by Sun et al. [48], Jamei et al. [42] and Balachandramohan et al. [49] who observed the presence of crystalline phases of both iron oxide (FeO) and iron (α-Fe). Some others peaks not attributed by Sun et al. in his diffraction patterns [48] are in fact due to the $Fe_3O_4$ presence. The oxide absence in our case is explained by the storage precautions in inert and dehydrated atmosphere taken to avoid the oxidation of such reactive nanoparticles. After one month exposition to air some $Fe_3O_4$ peaks combined with iron lines (α-Fe) appeared in the diffractogramms of all the samples regardless the variation of the preparation of the ZVI nanoparticles.

The strong broadening the α-Fe lines and the high level of the background noise is the signature of the nanometric particles occurrence. The size of the crystalline coherence domains (L) can be estimated from the Full Width at Half Maximum (FWHM) of the peaks by using the Scherrer equation:

$$L = 0.89 \times \frac{\lambda}{(\Delta(2\theta)\times\cos(\theta))} \quad \text{.....(8)}$$

where λ is the X-ray beam wavelength, $\theta$ is the diffraction angle, and ($2\theta$) can be taken as equal to the FWHM of the X-ray diffraction peak in radian. The size of the crystalline coherence domains (L) are equal to about 22 nm, 10 nm and 14 nm in $Fe^0$, $Fe^0$-UB and $Fe^0$-CHR, respectively. Thus, the broadening of the iron (α) *110*

diffraction peak of the ultrasonically prepared samples compared to the ones obtained in silent conditions indicates a decrease in the particle cristallinity attributed to the ultrasound treatment all along the reduction synthesis.
The physical effects of the ultrasound in a liquid medium include effective mass transfer through turbulent mixing and acoustic streaming increasing the reaction rate.
Jamei et al. [42] carried out an ultrasound-assisted reduction of iron (II) sulphate to ZVI nanoparticles by using an ultrasonic probe at 20 kHz. They have shown that average particle size was decreased under high precursor/reductant concentration or by increasing ultrasonic power by comparison with silent conditions. In agreement with this work X-ray diffraction results suggests that tiny crystallites were generated by using ultrasound irradiation acting as a nucleating agent and improving the dispersion so that a lot of crystallites nuclei were formed which tends to aggregate as increasing time.

*3.1.2. Infra-red spectroscopy*

All the spectra of Fig. 2 shows typical bands at about 470, and 626, for $Fe^0$-UB and $Fe^0$-CHR, which are quite similar to the bands founds in magnetite ($Fe_3O_4$) [50]. Additional bands at 540, and 700 $cm^{-1}$ are found in the $Fe^0$ spectrum, which are also observed in lepidocrocite (FeOOH) [50]. In fact all these peaks in the domain 400-700 $cm^{-1}$ are assigned to the Fe-O bonds vibrations. The Fe-O bonds were formed after the ZVI particles exposure to air and are the signature of the high reactivity with $O_2$ gas and humidity ($H_2O$) which is unavoidable when manipulating the nanoparticles in air.
The bands between 910 $cm^{-1}$ and 1400 $cm^{-1}$ can be attributed to the presence of hydrogenocarbonates ($HCO_3^-$) and carbonates ($CO_3^{2-}$) ions adsorbed on the surface of iron oxhydroxide [51-52], owing also to the contact with $CO_2$ from air and moisture. The peaks at about 910 $cm^{-1}$ could be attributed to the symmetric in-plane bending of $CO_3$. Moreover, the bands in the range 1010-1034 $cm^{-1}$ are assigned to C-OH stretching (in $HCO_3^{2-}$) and the ones in the range 1344-1400 $cm^{-1}$ are attributed $CO_3^{2-}$ symmetric stretching vibrations. The peak at 1633 $cm^{-1}$ is attributed to $CO_3^{2-}$ antisymmetric stretching vibrations (only appearing in $Fe^0$ sample).

The bands at about 2855-2888 $cm^{-1}$ are assigned to $CH_2$ symmetric stretching vibrations and the ones at 2927-2977 $cm^{-1}$ are attributed to $CH_2$ antisymmetric stretching vibrations. These two bands may be explained by the ethanol chemisorption at the surface of the iron nanoparticles after washing. The IR spectra of the ZVI nanoparticles (Fig. 2) show the presence of a strong absorption band at 3437 $cm^{-1}$ corresponding to the symmetrical O-H stretching vibration of the hydroxyl group. This band is assigned to the presence of adsorbed water at the ZVI nanoparticles surface. The O-H stretching vibration of the adsorbed water was also observed at about 1615 $cm^{-1}$.

*3.1.3. $N_2$ adsorption-desorption at 77 K*

The measured adsorption-desorption isotherms (Fig. 3) are typical of type IV isotherms with a $H_3$ hysteresis loops according to the IUPAC classification. This demonstates the presence of mesoporous pores (2 nm <Ø<50 nm) in which nitrogen liquid is condensed at 77 K. The BET specific surface areas ($S_{BET}$) of the $Fe^0$, $Fe^0$-UB and $Fe^0$-CHR prepared nanoparticles are 22 $m^2.g^{-1}$, 99 $m^2.g^{-1}$ and 145 $m^2.g^{-1}$, respectively. For comparison, $S_{BET}$ values given in the literature are between 20 $m^2.g^{-1}$ and 50 $m^2.g^{-1}$ for iron nanoparticles prepared in silent conditions [44, 53-55]. Assuming a spherical shape of non-aggregated nanoparticles, the particle diameter (d) can be determined from the $S_{BET}$, by the equation:

$$d = \frac{6}{(\rho \times S_{BET})} \quad \text{.....(9)}$$

where $\rho$ is the iron volumic mass (7.874 $g.cm^{-3}$). Thus, the calculated mean diameter of the $Fe^0$ and $Fe^0$-UB nanoparticles is about 35 nm and 8 nm, respectively, and close to the 22 nm and 10 nm values determined by X-ray diffraction. The difference between these two estimated values is explained by the slight aggregation of the $Fe^0$ and $Fe^0$-UB particles. In the case of $Fe^0$-CHR, a high disagreement is found between the diameter estimated from $S_{BET}$ (5 nm) and the one calculated from X-ray diffraction (14 nm). This disagreement is attributed to the high degree of clustering leading to a particular sample texture consisting of a porous arrangement of agglomerated particle aggregates.

Fig. 2S shows a predominance of mesopores (pore diameter in the range 2-50 nm). Moreover, the $Fe^0$-CHR pore volume is almost triple the one of $Fe^0$-UB which is

almost double the one of $Fe^0$. The mesoporous volume of the $Fe^0$, $Fe^0$-UB and $Fe^0$-CHR prepared nanoparticles are 0.09 $cm^3.g^{-1}$, 0.33 $cm^3.g^{-1}$ and 0.50 $cm^3.g^{-1}$, respectively.

The ultrasound-assisted synthesis of ZVI nanoparticles enables to obtain on one hand a smaller particle size (see XRD characterization), and on the other hand some larger pores volumes such as mesoporous ones which are cavities formed in between the nanoparticles aggregates. The pore volume is increasing while increasing the ultrasound power through ultrasound-assisted synthesis [56].

*3.1.4. SEM characterization*

The SEM images (Fig. 4) display two kinds of ZVI nanoparticles morphologies: chain and sheets. The elemental composition determined by EDX analysis (Fig. 4) of the various samples, indicates mainly the presence of Fe and O. The presence of O originates from the oxidation of the iron nanoparticles due to their reaction with $O_2$ from air. Whatever the preparation mode (conventional or ultrasound-assisted), the main presence of ZVI nanoparticles having a spherical shape and a chain texture (surrounded by red line in image C1) has been observed. This morphology type has been reported by many authors [57-58]. Regardless the preparation method, the single particle diameter size is of the order of 40 nm to 80 nm and higher than the elemental particles diameters determined from XRD or $S_{BET}$. The SEM images shows that the particles are often agglomerated either in the form of chains or in the form of few particles agglomerates. The particles chains are agglomerated together and formed a porous network.

Several clusters made of the agglomeration of few particles may come from the aggregation of nanoparticles due to their magnetic properties, this effect is more important in the case of $Fe^0$ prepared by the conventional method [59]. As mentioned by recent works [60-61] the limitation of the agglomeration is obtained by polymer coating of the ZVI nanoparticles. This suggests investigating as future prospects the effect of polymer stabilizers addition during the ZVI nanoparticles synthesis.

A sheet texture (red circle zones in Fig. 4, images a2 and b2) has been observed in $Fe^0$ and $Fe^0$-UB. The sheets are arranged in the form of “radiating plates” texture

agglomerates of 0.5 µm -1 µm dimension size. Such a texture was previously observed and attributed to the use of ultrasound-assisted method by Jamei et al. [42]. However, we have also observed the platelet texture formation through a conventional agitation synthesis. Other researchers have noted this phenomenon [62] and have attributed its occurence to the magnetic forces between the ZVI particles. Thus, it suggests that this texture may rather originate from solution inhomogeneities (crystallite germs) which might induce an oriented anisotropic germination.
By using a high ultrasonic power assisted synthesis, the solution has become more homogeneous preventing the development of such oriented growth. The SEM images of the $Fe^0$-CHR sample (as image c1 in Fig. 4) shows that the low frequency ultrasound-assisted production of ZVI nanoparticles allows to obtain more uniform and smaller spheres (40 nm diameter size) than by using conventional stirring or ultrasonic bath.

### *3.2. Removal of Cr(VI) ions*

#### *3.2.1. Cr(VI) removal in UHQ water*

##### *3.2.1.1. Effect of pH*

Cr(VI) removal pH dependence is illustrated in Fig.5. The $Fe^0$ removal efficiency is the lowest whereas $Fe^0$-CHR shows the highest Cr(VI) removal, especially at pH>3. The maximum removal is obtained at pH 2. The pH increase induces a decrease in Cr(VI) removal. Similar results have been reported [35, 42, 63-64]. This evolution is explained by the increase in the iron oxidation rate in the presence of a large $H^+$ amount (reaction 10) at pH<6 despite a strong corrosion. Cr(VI) speciation depends on the solution pH and on the aqueous concentration. At acidic pH (pH<6), $HCrO_4^-$ is the main Cr species, the reduction reaction is:

$$HCrO_4^- + Fe^{(0)} + 7\ H^+ \longrightarrow Fe^{3+} + Cr^{3+} + 4\ H_2O \quad \text{.....(10)}$$

At pH>6, $CrO_4^{2-}$ is the predominate species in water and the reduction reaction is:

$$CrO_4^{2-} + Fe^{(0)} + 4\ H_2O \longrightarrow Fe^{3+} + Cr^{3+} + 8\ OH^- \quad \text{.....(11)}$$

According to these equations (10 and 11), a mole of Fe(0) can reduce a mole of Cr(VI). Consequently, as the reaction is heterogeneous, an excess amount of Fe(0) must be

applied in order to completely reduce all Cr(VI) to Cr(III).

At alkaline pH, iron oxide layer and Fe(III)-Cr(III) oxy-hydroxides are formed:

$(1-x)\ Fe^{3+} + x\ Cr^{3+} + 2\ H_2O \longrightarrow Fe_{(1-x)}Cr_xOOH + 3\ H^+$ .....(12)

They cover the surface of the ZVI nanoparticles and play a role of physical barrier, reducing the particles reactive sites by blocking the Cr(VI) access to the nanoparticles surfaces. Similarly $Fe_{(2-x)}Cr_xO_4$ spinel type solid can be also formed. This can explain the decrease in the reduction reaction rate at more basic pH (11).

After treatment of the Cr(VI) solutions by $Fe^0$ nanoparticles at various pH, some solid particles were obtained by reaction of iron and its precipitation in various forms. These solids were firstly recovered by filtration of the Cr(VI) solutions after treatment by the $Fe^0$ nanoparticles, and secondly studied by XRD. The XRD pattern of the solid obtained at pH=4 (Fig. 6), indicates mainly the presence of iron with some small amounts of magnetite ($Fe_3O_4$) and lepidocrocite (FeOOH) owing to the ZVI nanoparticles oxidation. As increasing the pH up to 5, lepidocrocite is mainly formed by the $Fe^{2+}$ ions precipitation and the XRD lines intensities of chromite ($FeCr_2O_4$) or magnetite start to increase. The presence of lepidocrocite due to ZVI nanoparticles oxidation was also confirmed by infra-red characterization. As the chromite and the magnetite XRD peaks are almost at the same $2\theta$ positions, these lines might result from the formation of a $Fe^{(II)}Fe^{(III)}_{2-x}Cr^{(III)}_xO_4$ spinel structure demonstrating the Cr(VI) reduction after the treatment by ZVI nanoparticles. At pH 8 and 9, the diffractogramms show a mixture of lepidocrocite and spinel type structure (i.e. $Fe^{(II)}Fe^{(III)}_{2-x}\,Cr^{(III)}_xO_4$).

*3.2.1.2 Kinetics study*

At pH 2, the Cr(VI) ions removal by the prepared ZVI nanoparticles is rapid (Fig. 7). Whatever the stoichiometry of the three types of ZVI nanoparticles, the Cr(VI) reduction starts very quickly and then slows down. At the kinetics beginning, the Cr(VI) ions can easily access the surface of the fresh ZVI nanoparticles possessing a high reduction capacity. But as the reaction progresses, the nanoparticles surface reactive sites are gradually saturated. Increasing the concentration and decreasing the dose yields to slow the Cr(VI) ions removal. The complete Cr(VI) removal at 20 $mg.L^{-1}$ initial concentration can be attained after 40 min with a dose of 100 $mg.L^{-1}$ of

$Fe^0$-CHR nanoparticles (Fig 7 a). By contrast, according to Cissoko et al. [35] the total removal at pH 5.5 of the same Cr(VI) concentration requires a micrometric ZVI powder dose of 10 $g.L^{-1}$ during 2 hours. In agreement with our results, Montesinos et al. [37] have used a ZVI nanoparticles dose of about 0.05 $g.L^{-1}$ to fully reduce Cr(VI) initially at 15.6 $mg.L^{-1}$ after only 30 min (pH 3).

The pseudo first-order kinetic model has been applied to all the experimental data (Figures S3). This model was previously reported to describe the Cr(VI) removal kinetics by ZVI nanoparticles [43, 65-66]. According to this model, the following time dependence relation (13) can be established for the residual concentration:

$$\ln\left(\frac{C}{C_0}\right) = -kt \quad \text{.....(13)}$$

where $k$ is the pseudo first-order rate constant ($min^{-1}$), t the reaction time (min), and $C$ and $C_o$ represent the residual and the initial Cr(VI) concentrations ($mg.L^{-1}$), respectively.

While Fe(0) is in excess with respect to Cr(VI) (case of the dose equal to 100 $mg.L^{-1}$), the calculated parameters of this model (Table 2) indicate quite a satisfactory fitting ($R^2 > 0.87$). However, this model appears to be not reliable in the case of a 1/1 molar ratio stoichiometry of Fe(0)/Cr(VI) (when $C_{Cr(VI)}$=10 $mg.L^{-1}$ and the ZVI dose is 10 $mg.L^{-1}$). Furthermore, the pseudo first-order kinetic model better fits the experimental data for $Fe^0$ nanoparticles sample than for the ultrasonically synthesized nanoparticles (Figures S3).

Indeed, Fiúza et al. [36] have shown that the Cr(VI) reduction kinetic rate depended strongly on the ZVI particles surface characteristics and mainly on their superficial oxidation state and available surface area. These authors have applied the shrinking particle type model with a rate limitation by the surface reaction. In this model, the kinetic constant is proportional to the available iron surface area, to the initial volume of solution and to the chromium concentration. This model equation is:

$$1 - \left(\frac{C}{C_0}\right)^{\frac{1}{3}} = kt \quad \text{.....(14)}$$

where k is a kinetic parameter. It can also describes the heterogeneous reduction reactions kinetics (Figures S4, Table 2) but not at small dose of ZVI nanoparticles (i.e. 10 $mg.L^{-1}$).

Fig. 8 shows a linear growing relationship between the k reaction constants (from Table 2) and the various ZVI nanoparticles $S_{BET}$ whatever the studying conditions.

This confirms the proportionality of the Cr(VI) reduction rate to the particles active surface as for such an heterogeneous reaction.

*3.2.1.3. Cr(VI) removal in waste water compared to UHQ water*

Table 3, Table 4 and Fig. S5 confirm the better reduction efficiency of the $Fe^0$-CHR nanoparticles compared to the $Fe^0$ or $Fe^0$-UB ones for the treatment of either synthetic solutions (prepared in UHQ water) or industrial wastewater.
Table 3 allows comparing the treatments efficiencies by the ZVI nanoparticles in the same conditions (same iron dose, stirring mode and reaction time) for a synthetic solution (prepared with UHQ water) and for an industrial effluent (initial composition given in Table 1 of section 2.3) having exactly the same initial Cr(VI) concentration: 11.8 $mg.L^{-1}$. Table 3 (a) and Fig. S5 show that the Cr(VI) reduction in UHQ water is more effective as increasing the ZVI nanoparticles dose and as using the $Fe^0$-CHR nanoparticles. By treatment with the $Fe^0$-CHR sample, the removal efficiency has reached 94.3% and 50.8 % with a 0.6 $g.L^{-1}$ and 0.1 $g.L^{-1}$ dose, respectively.
For the industrial effluent treatment at same initial Cr(VI) concentration (i. e. 11.8 $mg.L^{-1}$), the Cr(VI) removal is less efficient than for the synthetic solution because of the presence of other metals which are also reduced by the ZVI nanoparticles (Table 3 (b)).
According to the $Zn^{2+}/Zn$ standard redox potential ($E°Zn^{2+}/Zn$ =-0.76 V) which is lower than the $Fe^{2+}/Fe$ one ($E°Fe^{2+}/Fe$ =-0.44 V), the $Zn^{2+}$ effluent concentration is not modified after the treatment by the ZVI nanoparticles. By contrast, owing to their redox potential higher than the $Fe^{2+}/Fe$ one, Cr(VI) ($E°CrO_4^{2-}/Cr^{3+}$=-0.11 V), Cu(II) ($E°Cu^{2+}/Cu$ =0.34V) and Ni(II) ions ($E°Ni^{2+}/Ni$ =-0.25V) are both reduced by the ZVI nanoparticles. As expected by the thermodynamics the Cr(VI) reduction is dominant (94.3% efficiency) with respect to the Ni(II) reduction for which the maximum efficiency is about 24% by using the $Fe^0$-CHR sample at 0.6 $g.L^{-1}$. The Ni(II) removal from aqueous medium by ZVI nanoparticles was previously reported [1]. The $Cu^{2+}$ ions initially at low concentration (1.27 $mg.L^{-1}$) are also reduced by $Fe^0$-CHR sample at 0.6 $g.L^{-1}$ with about 49% efficiency.

The absence of increase of the total iron ions concentration (Fe(II)+Fe(III)) after the industrial effluent treatment whatever the kind of nanoparticle confirms the solid state iron compounds precipitation. This might be in the form of lepidochrocite or spinel chromite for the synthetic solution treatment as evidenced by X-ray diffraction (cf. section 3.2.1.1).

Table 3 also displays an increase in the Cr(III) concentration (i.e. the Cr (VI) concentration subtracted from the $Cr_{total}$ one) following the trend of efficiency of the Cr(VI) removal by the various types of ZVI nanoparticles ($Fe^0$-CHR> $Fe^0$-UB> $Fe^0$). However, the Cr(III) concentration is always lower than the initial Cr(III) concentration indicating a decrease in agreement with a Cr(III) precipitation in form of solids such as chromite.

The Cr(VI) reduction to Cr(III) by reaction with ZVI nanoparticles yields to a pH increase noted in Table 3 (initial pH = 4.8), as expected by the (10) and (11) redox reactions. This pH increase is related to the ZVI particles dose yielding to their oxidation and to the precipitations of iron oxyhydroxides and iron oxides (such as lepidocrocite and magnetite). These precipitations make the pH more basic through acido-basic equilibriums established between solids and solution. After the synthetic solution treatment by the $Fe^0$-CHR sample, the pH has reached 5.3 and 8.2 by using a 0.1 $g.L^{-1}$ and 0.6 $g.L^{-1}$ dose, respectively. The treated industrial effluent pH (Table 3(b)) which depends also on the dissolved metallic species tends also to be basic after treatment by the $Fe^0$-CHR nanoparticles regardless of the dose.

The treatments were also tested on solutions of 0.14 $mg.L^{-1}$ Cr(VI) concentrations prepared either from UHQ water solution or from an industrial effluent. The concentrations measured after the reaction with ZVI nanoparticles (Table 4) demonstrate the treatment success allowing to obtain final Cr(VI) concentrations below the required standard for an effluent discharge the in environment (<50 $\mu g.L^{-1}$). Such wastewater treatments by ultrasonically prepared ZVI nanoparticles are expected to be efficient for tertiary treatments as for example to refine the Cr(VI) concentration after a metallic ions precipitation by lime addition.

## 4. Conclusion

As a conclusion, an ultrasound-assisted method was developed for the ZVI nanoparticles synthesis. The 20 kHz ultrasonication of iron(III) solutions with $NaBH_4$ reducer in a cup horn reactor has allowed to prepare almost spherical ZVI nanoparticles ($Fe^0$-CHR) with uniform size distribution (diameter of 40 nm). They are arranged in a chain aggregates morphology as observed by SEM and possess a high specific surface area (145 $m^2.g^{-1}$) compared to the ones prepared through mechanical stirring (22 $m^2.g^{-1}$).

Rapid Cr(VI) reduction kinetics with than 30 min or less contact time is required for treatments by such ZVI nanoparticles in pure water solutions. The more effective and faster Cr(VI) reduction in synthetic solutions by using the $Fe^0$-CHR ZVI nanoparticles rather than others is explained by their high porosity and specific surface area developed through the 20 kHz ultrasonic synthesis achieved in a cup horn reactor. Indeed, the Cr(VI) removal kinetics rate constants are linearly related to the BET surface areas of the ZVI nanoparticles.

The Cr(VI) removal kinetics are well fitted either by the pseudo first order model or the shrinking particle type model limited by a surface reaction when excess of ZVI nanoparticles is used with respect to Cr(VI).

The Cr(VI) anions were reduced to Cr(III) by heterogeneous reaction with ZVI nanoparticles. Further Cr(III) co-precipitation with iron cations (Fe(II)) in the form of chromite at pH>7 was evidenced by XRD characterization.

These ultrasonically prepared ZVI nanoparticles have proven to be very efficient for the Cr(VI) ions reduction either in UHQ water synthetic solutions or in effluent from metal surface processing industry, and even in the presence of other metal ions such as $Ni^{2+}$. The ZVI nanoparticles prepared by a 20 kHz ultrasonic probe have been found more effective in removing Cr(VI) ions than any kind of ZVI nanoparticles conventionally prepared. The control of the ZVI nanoparticles dose allows to decrease the Cr(VI) concentration in order to treat industrial effluent at the required environmental standards. Future prospects will concern the studies on the stabilization of these ultrasonically prepared ZVI nanoparticles in order to limit their efficiency loss through aging and their reactivity during users' manipulations.

# Credit author statement

Ms. Ref. No.: JECE-D-20-03844
Title: Improvement of zero valent iron nanoparticles by assisted-ultrasound synthesis, study of Cr(VI) removal and application for the treatment of metal surface processing wastewater
Journal of Environmental Chemical Engineer

**Declaration of interests**
The authors declare that they have no known competing financial interests or personal relationships that could have appeared to influence the work reported in this paper.

## Acknowledgement

The authors thanks the Ministry of Foreign Affair of France (Campus France) and the Ministry of Higher Education and Scientific Research of Algeria for awarding two scholarship programs to Nourhane Bounab: an Eiffel excellence scholarship and a Profas B+ grant, respectively.

## References

[1] L. Handojo, D. Pramudita, D. Mangindaan, A. Indarto, Application of Nanoparticles in Environmental Cleanup, in: R. Bharagava (Eds.), Emerging Eco-friendly Green Technologies for Wastewater Treatment, Microorganisms for Sustainability vol. 18, Springer, Singapore, 2020, pp. 45-76 https://doi.org/10.1007/978-981-15-1390-9.

[2] S. Comba, A. Di Molfetta, R. Sethi, A comparison between field applications of nano, micro-, and millimetric zero-valent iron for the remediation of contaminated aquifers, Water. Air. Soil. Pollut. 215 (2011) 595–607. https://doi.org /10.1007/s11270-010-0502-1.

[3] B.D. Yirsaw, M. Megharaj, Z. Chen, R. Naidu, Environmental application and ecological significance of nano-zero valent iron, J. Environ. Sci. (China). 44 (2016) 88–98. https://doi.org /10.1016/j.jes.2015.07.016.

[4] P. Westerhoff, Reduction of nitrate, bromate, and chlorate by zero valent iron

(Fe$^0$), J. Environ. Eng. 129 (2003) 10–16. https://doi.org/10.1061/(ASCE)0733-9372(2003)129:1(10).

[5] R.W. Gillham, S.F. O'Hannesin, Enhanced degradation of halogenated aliphatics by zero-valent iron, Ground Water. 32 (1994) 958–967. https://doi.org /10.1111/J.1745-6584.1994.tb00935.x.

[6] S. Nam, P.G. Tratnyek, Reduction of azo dyes with zero-valent iron, Water. Res. 34 (2000) 1837–1845. https://doi.org/10.1016/S0043-1354(99)00331-0.

[7] A.M. Azzam, S.T. El-Wakeel, B.B. Mostafa, M.F. El-Shahat, Removal of Pb, Cd, Cu and Ni from aqueous solution using nano scale zero valent iron particles, J. Environ. Chem. Eng. 4 (2016) 2196–2206. https://doi.org /10.1016/j.jece.2016.03.048.

[8] S.R. Kanel, B. Manning, L. Charlet, H. Choi, Removal of Arsenic(III) from groundwater by nanoscale zero-valent iron, Environ. Sci. Technol. 39 (2005) 1291–1298. https://doi.org/10.1021/es048991u.

[9] B.A. Manning, J.R. Kiser, H. Kwon, S.R. Kanel, Spectroscopic investigation of Cr(III)- and Cr(VI)-treated nanoscale zerovalent iron, Environ. Sci. Technol. 41 (2007) 586–592. https://doi.org/10.1021/ES061721M.

[10] D.W. Blowes, C.J. Ptacek, J.L. Jambor, In-situ remediation of Cr(VI)-contaminated groundwater using permeable reactive walls: Laboratory studies, Environ. Sci. Technol. 31 (1997) 3348–3357. https://doi.org/10.1021/ES960844b.

[11] T. Astrup, S.L.S. Stipp, T.H. Christensen, Immobilization of chromate from Coal Fly Ash Leachate using an attenuating barrier containing zero-valent iron, Environ. Sci. Technol. 34 (2000) 4163–4168. https://doi.org/10.1021/ES0009424.

[12] R.T. Wilkin, C. Su, R.G. Ford, C.J. Paul, Chromium-removal processes during groundwater remediation by a zerovalent iron permeable reactive barrier, Environ. Sci. Technol. 39 (2005) 4599–4605. https://doi.org/10.1021/ES050157X.

[13] M. Cieślak-Golonka, Toxic and mutagenic effects of chromium(VI), A review, Polyhedron. 15 (1996) 3667–3689. https://doi.org/10.1016/0277-5387(96)00141-6.

[14] WHO, World Health Organization, Guidelines for Drinking Water Quality, Word Health Organization, Geneva, 2011. pp. 668.

[15] E. Vaiopoulou, P. Gikas, Regulations for chromium emissions to the aquatic environment in Europe and elsewhere, Chemosphere. 254 (2020) 126876. https://doi.org/10.1016/j.chemosphere.2020.126876.

[16] Official Journal of the French Republic n°0234, October 6th 2017, "Arrêté du 24/08/17 modifiant dans une série d'arrêtés ministériels les dispositions relatives aux rejets de substances dangereuses dans l'eau en provenance des installations classées pour la protection de l'environnement". https://www.legifrance.gouv.fr/eli/arrete/2017/8/24/TREP1713284A/jo/texte, (accessed 31 October 2010).

[17] Official Journal of the Algerian Republic n° 36 June 21st 2009, "Décret exécutif n° 9-209 Valeurs limites maximales de la teneur en substances nocives des eaux usées autres que domestiques au moment de leur déversement dans un réseau public d'assainissement ou dans une station d'épuration". https://www.joradp.dz/FTP/jo-francais/2009/F2009036.pdf, (accessed 31 October 2010).

[18] F. Gode, E. Pehlivan, Removal of Cr(VI) from aqueous solution by two Lewatit-anion exchange resins, J. Hazard. Mater. 119 (2005) 175–182. https://doi.org/10.1016/j.jhazmat.2004.12.004.

[19] S. Edebali, E. Pehlivan, Evaluation of Amberlite IRA96 and Dowex 1×8 ion-exchange resins for the removal of Cr(VI) from aqueous solution, Chem. Eng. J. 161 (2010) 161–166. https://doi.org/10.1016/j.ceJ.2010.04.059.

[20] A.P. Padilla, E.L. Tavani, Treatment of an industrial effluent by reverse osmosis, Desalination. 126 (1999) 219–226.https://doi.org/10.1016/S0011-9164(99)00178-2.

[21] G. Chen, C. Qiao, Y. Wang, J. Yao, Synthesis of magnetic gelatin and its adsorption property for Cr(VI), Ind. Eng. Chem. Res. 53 (2014) 15576–15581. https://doi.org/10.1021/IE502709u.

[22] C.E. Barrera-Díaz, V. Lugo-Lugo, B. Bilyeu, A review of chemical, electrochemical and biological methods for aqueous Cr(VI) reduction, J. Hazard. Mater. 223–224 (2012) 1–12. https://doi.org/10.1016/j.jhazmat.2012.04.054.

[23] M. Rivero-Huguet, W.D. Marshall, Reduction of hexavalent chromium mediated by micron- and nano-scale zero-valent metallic particles, J. Environ. Monitor. 11 (2009) 1072–1079. https://doi.org/10.1039/B819279K.

[24] S.W. Ali, M.L. Mirza, T.M. Bhatti, Removal of Cr(VI) using iron nanoparticles supported on porous cation-exchange resin, Hydrometallurgy. 157 (2015) 82–89. https://doi.org/10.1016/j.hydromet.2015.07.013.

[25] G. Qu, L. Kou, T. Wang, D. Liang, S. Hu, Evaluation of activated carbon fiber supported nanoscale zero-valent iron for chromium(VI) removal from groundwater in a permeable reactive column, J. Environ. Manage. 201 (2017) 378–387. https://doi.org/10.1016/j.jenvmaN.2017.07.010.

[26] G. Vilardi, T. Mpouras, D. Dermatas, N. Verdone, A. Polydera, L. Di Palma, Nanomaterials application for heavy metals recovery from polluted water: The combination of nano zero-valent iron and carbon nanotubes. Competitive adsorption non-linear modelling, Chemosphere. 201 (2018) 716–729. https://doi.org/10.1016/j.chemosphere.2018.03.032.

[27] H. Dong, J. Deng, Y. Xie, C. Zhang, Z. Jiang, Y. Cheng, K. Hou, G. Zeng, Stabilization of nanoscale zero-valent iron (nZVI) with modified biochar for Cr(VI)

removal from aqueous solution, J. Hazard. Mater. 332 (2017) 79–86. https://doi.org/10.1016/j.jhazmat.2017.03.002.

[28] L. Qian, W. Zhang, J. Yan, L. Han, Y. Chen, D. Ouyang, M. Chen, Nanoscale zero-valent iron supported by biochars produced at different temperatures: Synthesis mechanism and effect on Cr(VI) removal, Environ. Pollut. 223 (2017) 153–160. https://doi.org/10.1016/j.envpol.2016.12.077.

[29] R. Fu, Y. Yang, Z. Xu, X. Zhang, X. Guo, D. Bi, The removal of chromium(VI) and lead(II) from groundwater using sepiolite-supported nanoscale zero-valent iron (S-NZVI), Chemosphere. 138 (2015) 726–734. http://doi.org/10.1016/j.chemosphere.2015.07.051.

[30] L. Shi, X. Zhang, Z. Chen, Removal of chromium(VI) from wastewater using bentonite-supported nanoscale zero-valent iron, Water. Res. 45 (2011) 886–892. https://doi.org/10.1016/J.WATRES.2010.09.025.

[31] Z.-H. Diao, X.-R. Xu, H. Chen, D. Jiang, Y.-X. Yang, L.-J. Kong, Y.-X. Sun, Y.-X. Hu, Q.-W. Hao, L. Liu, Simultaneous removal of Cr(VI) and phenol by persulfate activated with bentonite-supported nanoscale zero-valent iron: Reactivity and mechanism, J. Hazard. Mater. 316 (2016) 186–193. https://doi.org /10.1016/j.jhazmat.2016.05.041.

[32] R. Zhao, Z. Zhou, X. Zhao, G. Jing, Enhanced Cr(VI) removal from simulated electroplating rinse wastewater by amino-functionalized vermiculite-supported nanoscale zero-valent iron, Chemosphere. 218 (2018) 458–467. https://doi.org /10.1016/j.chemosphere.2018.11.118.

[33] A. Özer, H.S. Altundoğan, M. Erdem, F. Tümen, A study on the Cr(VI) removal from aqueous solutions by steel wool, Environ. Pollut. 97 (1997) 107–112. https://doi.org/10.1016/S0269-7491(97)00065-1.

[34] M. Gheju, Hexavalent Chromium Reduction with Zero-Valent Iron (ZVI) in

Aquatic Systems, Water. Air. Soil. Pollut. 222 (2011) 103–148. https://doi.org /10.1007/s11270-011-0812-y.

[35] N. Cissoko, Z. Zhang, J. Zhang, X. Xu, Removal of Cr(VI) from simulative contaminated groundwater by iron metal, Process Saf. Environ. Protect. 87 (2009) 395–400. https://doi.org/10.1016/j.psep.2009.07.001.

[36] A. Fiúza, A. Silva, G. Carvalho, A.V. de la Fuente, C. Delerue-Matos, Heterogeneous kinetics of the reduction of chromium(VI) by elemental iron, J. Hazard. Mater. 175 (2010) 1042–1047. https://doi.org/10.1016/j.jhazmat.2009.10.116.

[37] V.N. Montesinos, N. Quici, E.B. Halac, A.G. Leyva, G. Custo, S. Bengio, G. Zampieri, M.I. Litter, Highly efficient removal of Cr(VI) from water with nanoparticulated zerovalent iron: understanding the Fe(III)–Cr(III) passive outer layer structure, Chem. Eng. J. 244 (2014) 569–575. https://doi.org /10.1016/j.cej.2014.01.093.

[38] Q. Zhang, D. Zhao, S. Feng, Y. Wang, J. Jin, A. Alsaedi, T. Hayat, C. Chen, Synthesis of nanoscale zero-valent iron loaded chitosan for synergistically enhanced removal of U(VI) based on adsorption and reduction, J. Colloid. Interf. Sci. 552 (2019) 735–743. https://doi.org/10.1016/j.jcis.2019.05.109.

[39] A. Rana, N. Kumari, M. Tyagi, S. Jagadevan, Leaf-extract mediated zero-valent iron for oxidation of Arsenic(III): Preparation, characterization and kinetics, Chem. Eng. J. 347 (2018) 91–100. https://doi.org/10.1016/j.cej.2018.04.075.

[40] C.P. Devatha, A.K. Thalla, S.Y. Katte, Green synthesis of iron nanoparticles using different leaf extracts for treatment of domestic waste water, J. Clean. Prod. 139 (2016) 1425–1435. https://doi.org/10.1016/j.jclepro.2016.09.019.

[41] M. Stefaniuk, P. Oleszczuk, Y.S. Ok, Review on nano zerovalent iron (nZVI): From synthesis to environmental applications, Chem. Eng. J. 287 (2016) 618–632.

https://doi.org/10.1016/j.ceJ.2015.11.046.

[42] M.R. Jamei, M.R. Khosravi, B. Anvaripour, A novel ultrasound assisted method in synthesis of nZVI particles, Ultrason. Sonochem. 21 (2014) 226–233. https://doi.org/10.1016/j.ultsonch.2013.04.015.

[43] X. Zhou, B. Lv, Z. Zhou, W. Li, G. Jing, Evaluation of highly active nanoscale zero-valent iron coupled with ultrasound for chromium(VI) removal, Chem. Eng. J. 281 (2015) 155–163. https://doi.org/10.1016/j.ceJ.2015.06.089.

[44] C.-B. Wang, W. Zhang, Synthesizing nanoscale iron particles for rapid and complete dechlorination of TCE and PCBs, Environ. Sci. Technol. 31 (1997) 2154–2156. https://doi.org/10.1021/es970039c.

[45] J. Andrieux, Stockage de l'hydrogène dans les borohydrures alcalins : hydrolyse du borohydrure de sodium, Ph. D Thesis, Université Claude Bernard- Lyon I, France, 2009.

[46] R.F. Contamine, A.M. Wilhelm, J. Berlan, H. Delmas, Power measurement in sonochemistry, Ultrason. Sonochem. 2 (1995) S43–S47. https://doi.org /10.1016/1350-4177(94)00010-P.

[47] J. Rodier, C. Bazin, J.P. Broutin, P. Chambon, H. Champsaur, L. Rodi, L'analyse de l'eau, eaux naturelles, eaux résiduaires, eau de mer, 8ème Edition, Dunod, Paris, 1996.

[48] Y.-P. Sun, X. Li, J. Cao, W. Zhang, H.P. Wang, Characterization of zero-valent iron nanoparticles, Adv. Colloid. Interface. Sci. 120 (2006) 47–56. https://doi.org /10.1016/j.cis.2006.03.001.

[49] J. Balachandramohan, T. Sivasankar, Ultrasound assisted synthesis of guar gum-zero valent iron nanocomposites as a novel catalyst for the treatment of

pollutants, Carbohydr. Polym. 199 (2018) 41–50. https://doi.org/10.1016/j.carbpol.2018.06.097.

[50] M. Veneranda, J. Aramendia, L. Bellot-Gurlet, P. Colomban, K. Castro, J. M. Madariaga, FTIR spectroscopic semi-quantification of iron phases: A new method to evaluate the protection ability index (PAI) of archaeological artefacts corrosion systems. Corros. Sci. 133 (2018) 68–77. https://doi.org /10.1016/j.corsci.2018.01.016.

[51] C. Su, D. L. Suarez, In situ infrared speciation of adsorbed carbonate on aluminium and iron oxides, Clays. Clay. Miner. 45 (1997) 814–825. https://doi.org/10.1346/CCMN.1997.0450605.

[52] G. Lefèvre, In situ Fourier-transform infrared spectroscopy studies of inorganic ions adsorption on metal oxides and hydroxides, Adv. Colloid. Interface. Sci. 107 (2004) 109–123. https://doi.org/10.1016/j.cis.2003.11.002.

[53] Q. Wang, S.R. Kanel, H. Park, A. Ryu, H. Choi, Controllable synthesis, characterization, and magnetic properties of nanoscale zerovalent iron with specific high Brunauer–Emmett–Teller surface area, J. Nanopart. Res. 11 (2008) 749–755. https://doi.org/10.1007/s11051-008-9524-7.

[54] Z. Fang, J. Chen, X. Qiu, X. Qiu, W. Cheng, L. Zhu, Effective removal of antibiotic metronidazole from water by nanoscale zero-valent iron particles, Desalination. 268 (2011) 60–67. https://doi.org/10.1016/j.desal.2010.09.051.

[55] D. Chen, K. Yang, H. Wang, J. Zhou, H. Zhang, Cr(VI) removal by combined redox reactions and adsorption using pectin-stabilized nanoscale zero-valent iron for simulated chromium contaminated water, RSC. Adv. 5 (2015) 65068–65073. https://doi.org/10.1039/C5RA10573K.

[56] Q. Chen, H. Ge, C. Yang, S. Lin, C. Fan, Study on pores in ultrasonic-assisted TIG Weld of Aluminum Alloy, J. Met. 7 (2017) 53.

https://doi.org/10.3390/met7020053.

[57] H.-S. Kim, T. Kim, J.-Y. Ahn, K.-Y. Hwang, J.-Y. Park, T.-T. Lim, I. Hwang, Aging characteristics and reactivity of two types of nanoscale zero-valent iron particles ($Fe^{BH}$ and $Fe^{H_2}$) in nitrate reduction, Chem. Eng. J. 197 (2012) 16–23. https://doi.org/10.1016/j.cej.2012.05.018.

[58] D. Lin, Z. Zhang, L. Hu, Adsorption Models of Groundwater Remediation by Nanoscale Zero Valent Iron. Proceedings of the 8th International Congress on Environmental Geotechnics, 1 (2018) 512–520. https://doi.org/10.1007/978-981-13-2221-1_55.

[59] D. Rosická, J. Šembera, Influence of structure of iron nanoparticles in aggregates on their magnetic properties, Nanoscale. Res. Lett. 6 (2011) 527. https://doi.org/10.1186/1556-276X-6-527.

[60] A. Galdames , L. Ruiz-Rubio, M. Orueta , M. Sánchez-Arzalluz,J. L. Vilas-Vilela, Zero-Valent Iron Nanoparticles for Soil and Groundwater Remediation, Int. J. Environ. Res. Public Health 17 (2020) 5817. https://doi.org/10.3390/ijerph17165817.

[61] H.M. Ibrahim, M. Awad, A.S. Al-Farraj, A.M. Al-Turki, Stability and Dynamic Aggregation of Bare and Stabilized Zero-Valent Iron Nanoparticles under Variable Solution Chemistry, Nanomaterials 10 (2020) 192. https://doi.org/10.3390/nano10020192.

[62] E.S. Yusmartini, D. Setiabudidaya, Ridwan, Marsi, Faizal, Synthesis and characterization of zero-valent iron nanoparticles, Adv. Mat. Res. 1112 (2015) 62–65. https://doi.org/10.4028/www.scientific.net/AMR.1112.62.

[63] L. Alidokht, A. Khataee, A. Reyhanitabar, S. Oustan, Reductive removal of Cr(VI) by tarch-stabilized $Fe^0$ nanoparticles in aqueous solution, Desalination. 270 (2011) 105-110. https://doi.org/10.1016/j.desal.2010.11.028.

[64 61] Y. Li, J. Li, Y. Zhang, Mechanism insights into enhanced Cr(VI) removal using nanoscale zerovalent iron supported on the pillared bentonite by macroscopic and spectroscopic studies, J. Hazard. Mater. 227–228 (2012) 211–218. https://doi.org/10.1016/j.jhazmat.2012.05.034.

[65] A.R. Esfahani, S. Hojati, A. Azimi, L. Alidokht, A. Khataee, M. Farzadian, Reductive removal of hexavalent chromium from aqueous solution using sepiolite-stabilized zero-valent iron nanoparticles: Process optimization and kinetic studies. Korean J. Chem. Eng. 31 (2014) 630–638. https://doi.org/10.1007/s11814-013-0285-3.

[66] Z. Peng, C. Xiong, W. Wang, F. Tan, Y. Xu, X. Wang, X. Qiao, Facile modification of nanoscale zero-valent iron with high stability for Cr(VI) remediation, Sci. Total. Environ. 596–597 (2017) 266–273. https://doi.org/10.1016/j.scitotenv.2017.04.121.

**Figure Caption**

Figure 1: X-ray diffractograms of $Fe^0$, $Fe^0$-UB and $Fe^0$-CHR samples

Figure 2: FTIR spectra of $Fe^0$, $Fe^0$-UB and $Fe^0$-CHR samples

Figure 3: $N_2$ adsorption-desorption isotherms at 77K of $Fe^0$, $Fe^0$-UB and $Fe^0$-CHR samples.

Figure 4: SEM images and EDX spectra of the iron nanoparticles: (a) $Fe^0$ , (b) $Fe^0$-UB and (c) $Fe^0$-CHR.

Figure 5: Effect of solution pH on Cr(VI) removal by $Fe^0$ prepared nanoparticles ($C_{Cr(VI)}$ = 10 $mg.L^{-1}$ ; nanoparticles dose = 100 $mg.L^{-1}$ ; t = 60 min).

Figure 6: X-ray diffraction spectra of $Fe^0$ sample after reaction with Cr(VI) at different pH values ($C_{Cr(VI)}$ = 10 $mg.L^{-1}$ ; $Fe^0$ dose = 100 $mg.L^{-1}$).

Figure 7: Kinetics of Cr(VI) removal at various initial concentration by $Fe^0$, $Fe^0$-UB and $Fe^0$-CHR samples at a dose of 100 $mg.L^{-1}$ (a, b) and 10 $mg.L^{-1}$ (c) (pH = 2).

Figure 8: Reaction constant k as a function of $S_{BET}$ for the different types of nanoparticles.

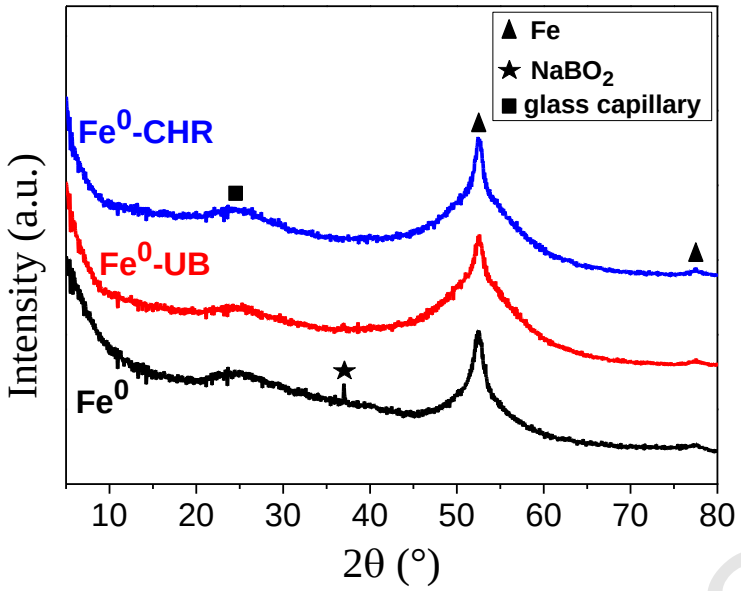


Figure 1: X-ray diffractograms of Fe$^0$, Fe$^0$-UB and Fe$^0$-CHR samples.

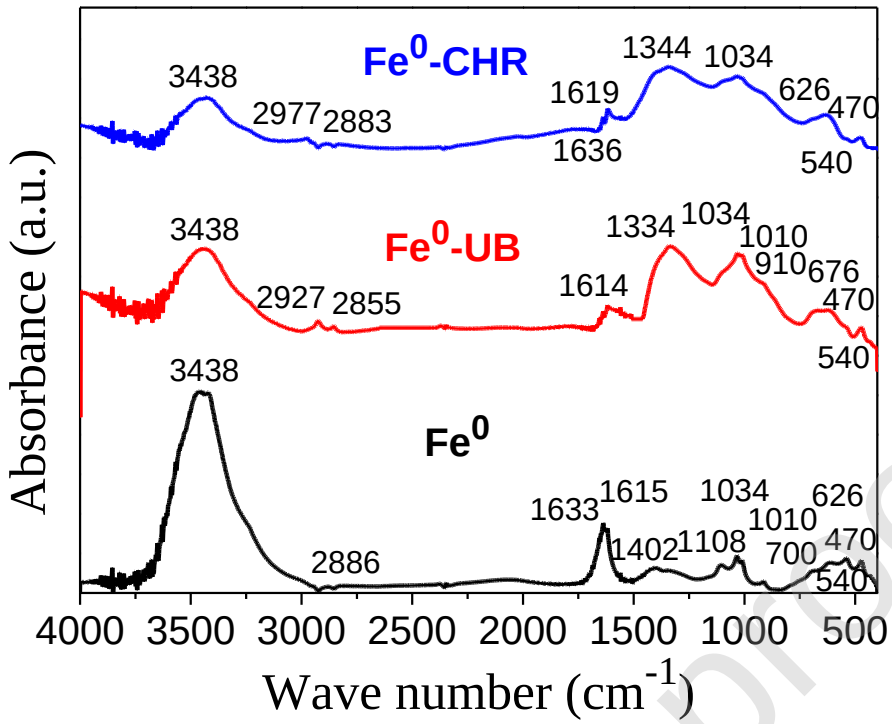


Figure 2: FTIR spectra of Fe$^0$, Fe$^0$-UB and Fe$^0$-CHR samples.

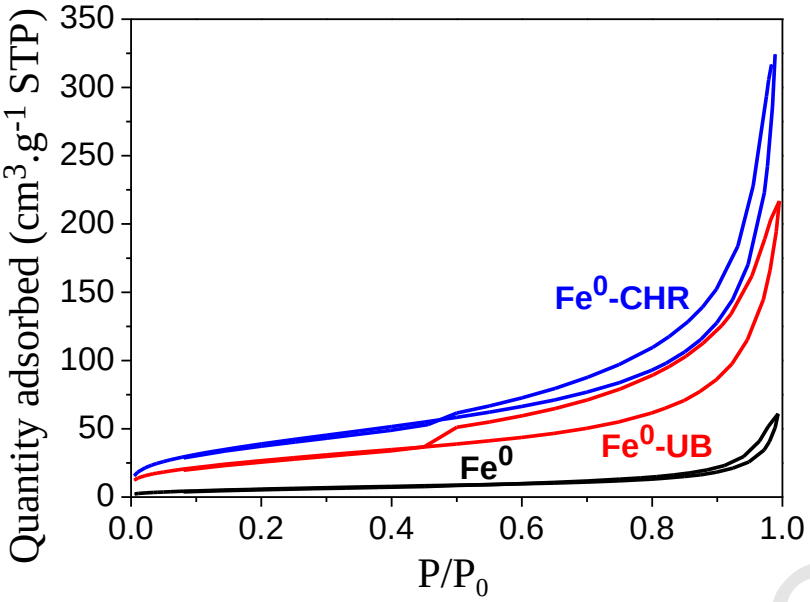


Figure 3: $N_2$ adsorption-desorption isotherms at 77K of $Fe^o$, $Fe^o$-UB and $Fe^o$-CHR samples.

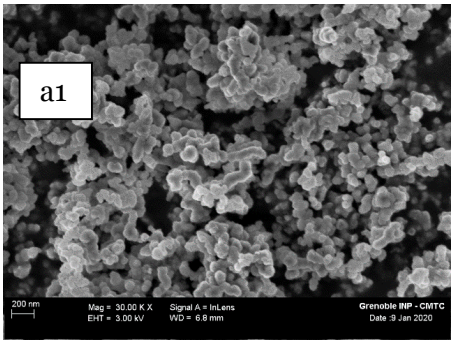


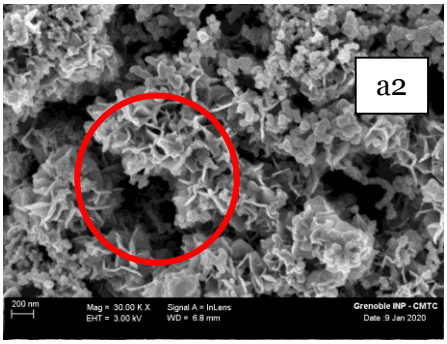


a3

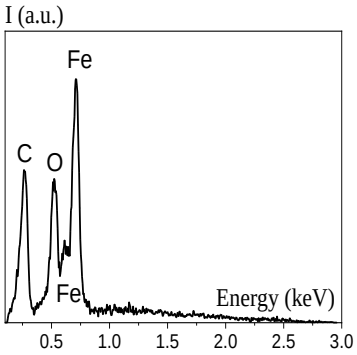


b1

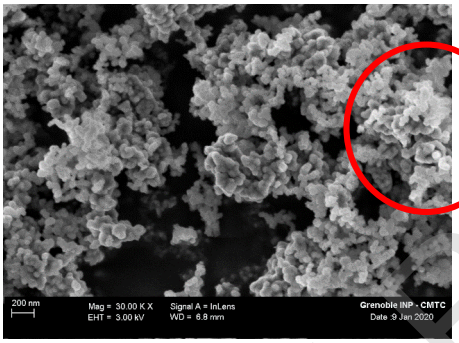


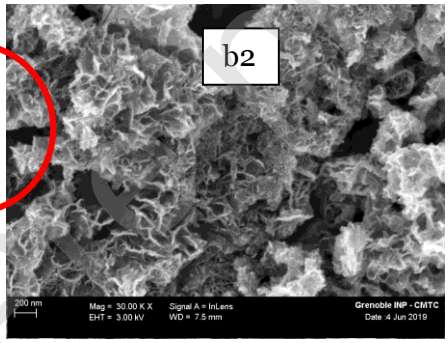


b3

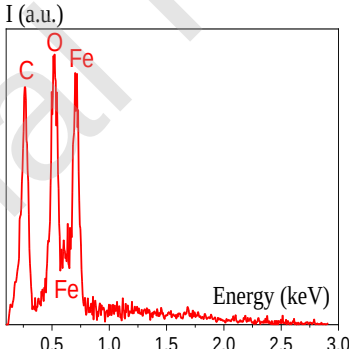


c1

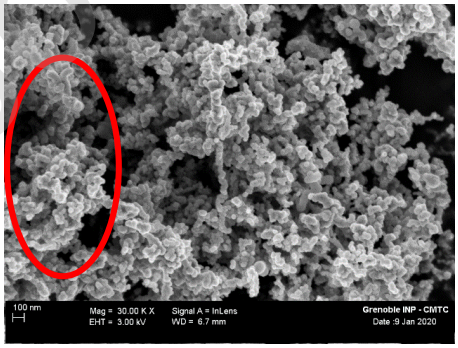


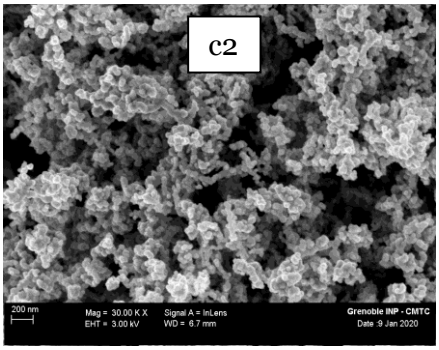


c3

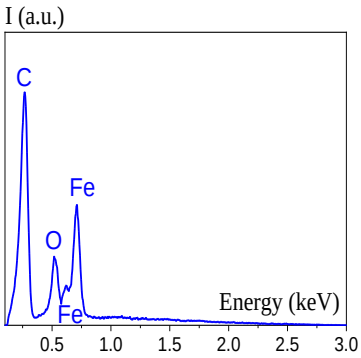


Figure 4: SEM images and EDX spectra of the iron nanoparticles: (a) $Fe^{o}$ , (b) $Fe^{o}$-UB and (c) $Fe^{o}$-CHR.

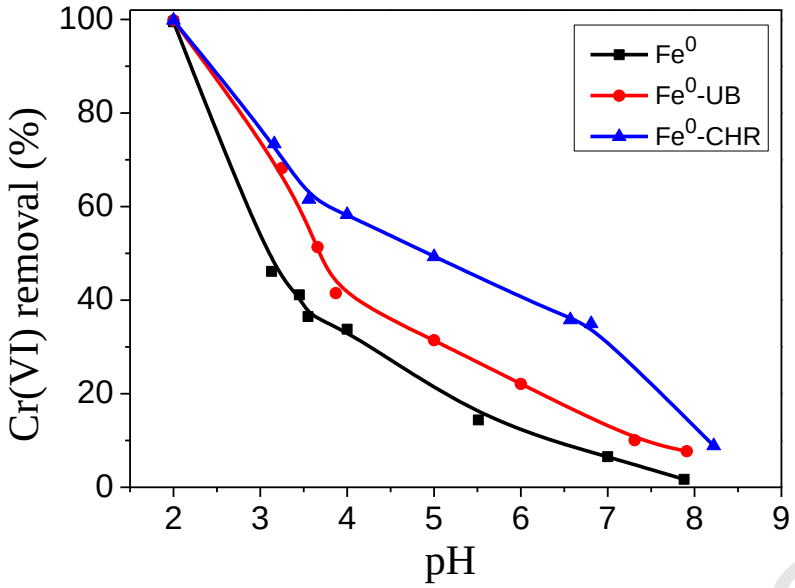


Figure 5: Effect of solution pH on Cr(VI) removal by Fe⁰ prepared nanoparticles ($C_{Cr(VI)}$ = 10 mg.L$^{-1}$ ; nanoparticles dose = 100 mg.L$^{-1}$ ; t = 60 min).

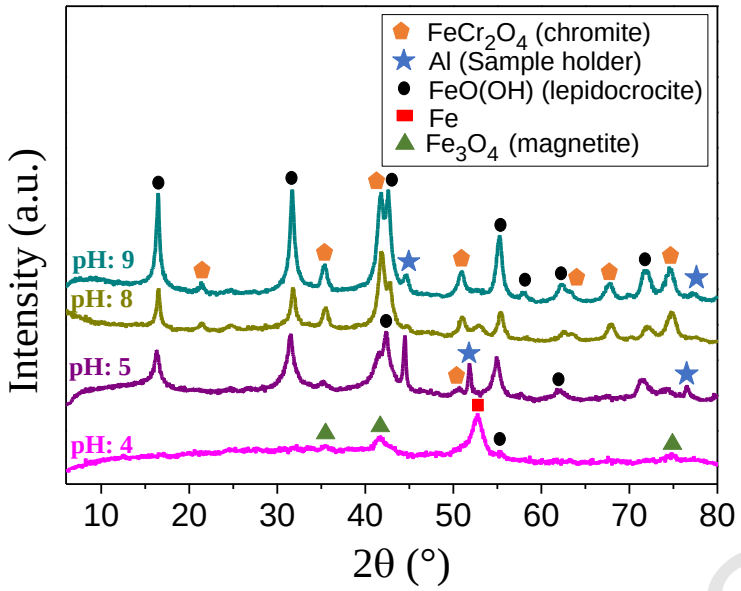


Figure 6: X-ray diffraction spectra of $Fe^0$ sample after reaction with Cr(VI) at different pH values ($C_{Cr(VI)}$ = 10 mg.L$^{-1}$ ; $Fe^0$ dose = 100 mg.L$^{-1}$).

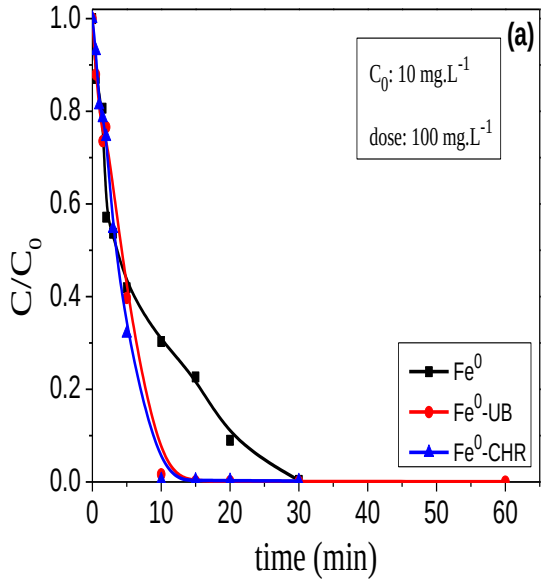


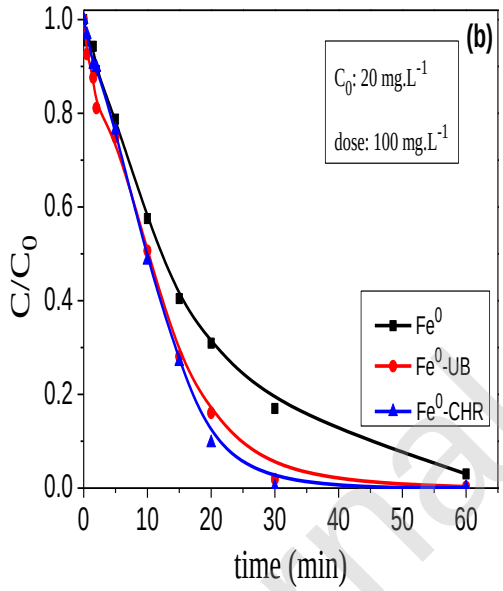

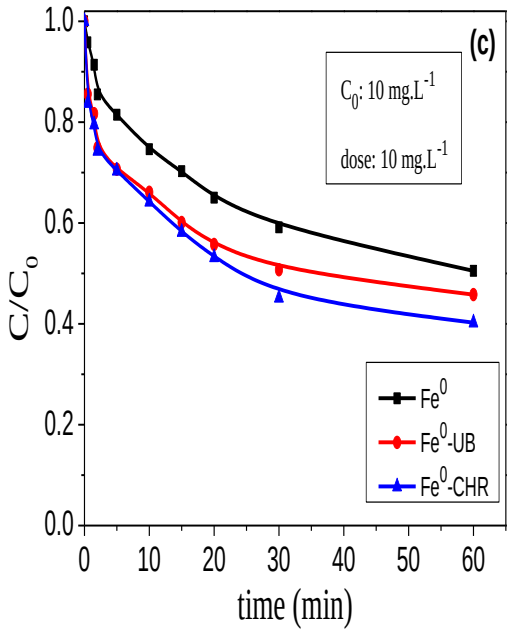


Figure 7: Kinetics of Cr(VI) removal at various initial concentration by Fe°, Fe°-UB and Fe°-CHR samples at a dose of 100 mg.L$^{-1}$ (a, b) and 10 mg.L$^{-1}$ (c) (pH = 2).

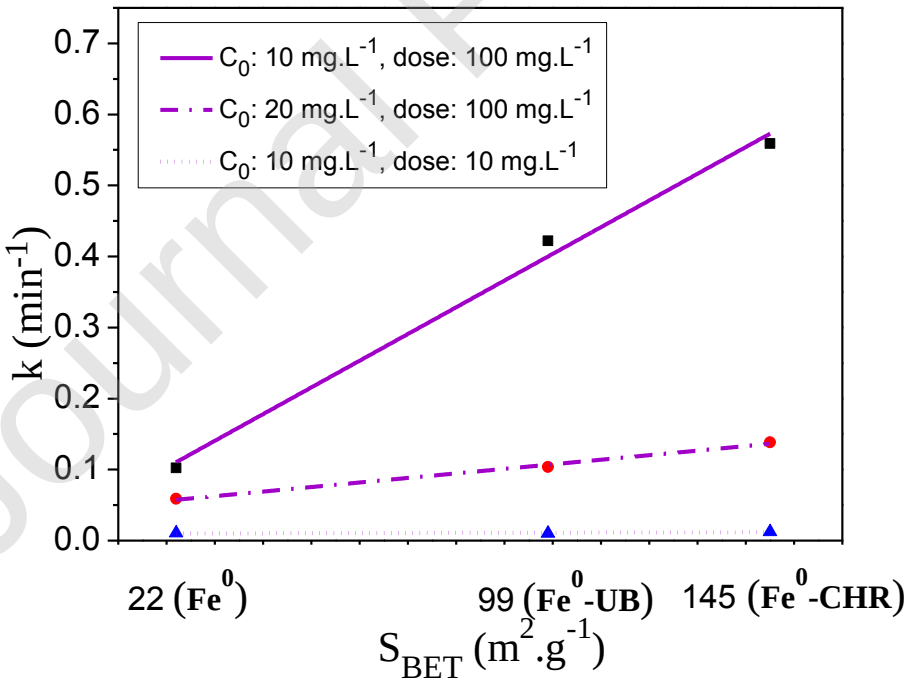

Figure 8: Reaction constant k as a function of $S_{BET}$ for the different types of nanoparticles.

Table 1 : Results of the wastewater analysis and its dilution*.

| pH | COD ($mg.L^{-1}$) | $Cr_{total}$ ($mg.L^{-1}$) | Cr(VI) ($mg.L^{-1}$) | Zn(II) ($mg.L^{-1}$) | Ni(II) ($mg.L^{-1}$) | $Fe_{total}$ ($mg.L^{-1}$) | Cu(II) ($mg.L^{-1}$) |
|---|---|---|---|---|---|---|---|
| 4.8 | 4.21 | 19.17 | 11.80 | 0.95 | 68.96 | 0.012 | 1.27 |
| 5.3* | 0.042* | 0.17* | 0.14* | 0.01* | 0.68* | <0.01* | <0.01* |

*diluted effluent about 1/100

Table 2. Summary of kinetic parameters of the pseudo-first order model (k: reaction constant in $min^{-1}$ and $R^2$ linear regression coefficient) for the Cr(VI) removal.

| | Prepared nanoparticles | | | | | |
|---|---|---|---|---|---|---|
| Conditions | Pseudo first-order model | | | $1-(C/C_o)^{(1/3)}=kt$ | | |
| | $Fe^o$ | $Fe^o$-UB | $Fe^o$-CHR | $Fe^o$ | $Fe^o$-UB | $Fe^o$-CHR |
| $C_{Cr(VI)}$: 10 $mg.L^{-1}$ Fe dose: 100 $mg.L^{-1}$ | $R^2$= 0.946 k= 0.1022 $min^{-1}$ | $R^2$= 0.903 k= 0.4219 $min^{-1}$ | $R^2$= 0.906 k= 0.5591 $min^{-1}$ | $R^2$= 0.929 k= 0.0230 $min^{-1}$ | $R^2$= 0.963 k= 0.0747 $min^{-1}$ | $R^2$= 0.980 k= 0.0855 $min^{-1}$ |
| $C_{Cr(VI)}$: 20 $mg.L^{-1}$ Fe dose: 100 $mg.L^{-1}$ | $R^2$= 0.999 k= 0.0587 $min^{-1}$ | $R^2$= 0.961 k= 0.1037 $min^{-1}$ | $R^2$= 0.870 k= 0.1383 $min^{-1}$ | $R^2$= 0.992 k= 0.0152 $min^{-1}$ | $R^2$= 0.991 k= 0.0237 $min^{-1}$ | $R^2$= 0.986 k= 0.0292 $min^{-1}$ |
| $C_{Cr(VI)}$: 10 $mg.L^{-1}$ Fe dose: 10 $mg.L^{-1}$ | $R^2$= 0.874 k= 0.0104 $min^{-1}$ | $R^2$= 0.803 k= 0.0102 $min^{-1}$ | $R^2$= 0.851 k= 0.0123 $min^{-1}$ | $R^2$= 0.906 k= 0.0051 $min^{-1}$ | $R^2$= 0.811 k= 0.0057 $min^{-1}$ | $R^2$= 0.860 k= 0.0064 $min^{-1}$ |

Table 3. Residual Cr(VI), total Cr, and others metals concentrations(mg.L$^{-1}$) after a 60 min treatment at 22°C by the three types of ZVI nanoparticles ($Fe^0$, $Fe^0$-UB, and $Fe^0$-CHR) at 0.1 g.L$^{-1}$ or 0.6 g.L$^{-1}$ dose of : (a) UHQ water solution, and (b) : industrial effluent ; at the same at initial Cr(VI) concentrations ($C_{o\ Cr(VI)}$=11.80 mg.L$^{-1}$).

(a) UHQ water, $C_{o\ Cr(VI)}$: 11.80 mg.L$^{-1}$

| dose | 0.1 g.L$^{-1}$ | | | 0.6 g.L$^{-1}$ | | |
|---|---|---|---|---|---|---|
| Iron nanoparticles | $Fe^0$ | $Fe^0$-UB | $Fe^0$-CHR | $Fe^0$ | $Fe^0$-UB | $Fe^0$-CHR |
| Cr(VI) | 9.46 | 9.08 | 5.80 | 7.32 | 3.51 | 0.67 |
| $Cr_{total}$ | 11.43 | 11.15 | 8.77 | 8.19 | 6.40 | 4.09 |
| pH | 6.5 | 5.5 | 5.3 | 8.7 | 8.4 | 8.2 |

(b) Industrial effluent, $C_{o\ Cr(VI)}$: 11.80 mg.L$^{-1}$, $C_{o\ Cr(III)}$: 7.37 mg.L$^{-1}$, $C_{o\ Ni(II)}$: 68.96 mg.L$^{-1}$

| dose | 0.1 g.L$^{-1}$ | | | 0.6 g.L$^{-1}$ | | |
|---|---|---|---|---|---|---|
| ZVI nanoparticles | $Fe^0$ | $Fe^0$-UB | $Fe^0$-CHR | $Fe^0$ | $Fe^0$-UB | $Fe^0$-CHR |
| Cr(VI) | 10.50 | 10.01 | 8.89 | 7.79 | 3.72 | 1.84 |
| $Cr_{total}$ | 12.80 | 12.65 | 12.06 | 8.32 | 4.46 | 2.04 |
| Ni(II) | 66.40 | 65.86 | 63.40 | 63.57 | 61.67 | 51.95 |
| $Fe_{total}$ | 0.01 | 0.05 | 0.01 | 0.01 | 0.01 | 0.04 |
| Zn(II) | 0.88 | 0.84 | 0.86 | 0.50 | 0.49 | 0.48 |
| Cu(II) | 1.14 | 1.10 | 1.07 | 0.88 | 0.87 | 0.65 |
| pH | 5.7 | 6 | 7.5 | 6.3 | 6.7 | 7.8 |

Table 4. Residual Cr(VI), total Cr, and others metals concentrations(mg.L$^{-1}$) after a 60 min treatment at 22°C by the three types of ZVI nanoparticles ($Fe^0$, $Fe^0$-UB, and $Fe^0$-CHR) at 0.1 g.L$^{-1}$ dose of : (a) UHQ water solution, and (b) : industrial effluent ; at the same at initial Cr(VI) concentrations ($C_{o\ Cr(VI)}$=0.14 mg.L$^{-1}$).

(a) UHQ water, $C_{o\ Cr(VI)}$: 0.14 mg.L$^{-1}$ ,

| dose | 0.1 g.L$^{-1}$ | | |
|---|---|---|---|
| Iron nanoparticles | $Fe^0$ | $Fe^0$-UB | $Fe^0$-CHR |
| Cr(VI) | 0.089 | 0.02 | 0.016 |
| $Cr_{total}$ | 0.09 | 0.06 | 0.03 |
| pH | 7.8 | 6.4 | 5.9 |

(b) Industrial effluent, $C_{o\ Cr(VI)}$: 0.14 mg.L$^{-1}$

| dose | 0.1 g.L$^{-1}$ | | |
|---|---|---|---|
| Iron nanoparticles | $Fe^0$ | $Fe^0$-UB | $Fe^0$-CHR |
| Cr(VI) | 0.006 | 0.0055 | 0.004 |
| $Cr_{total}$ | 0.03 | 0.01 | 0.01 |
| Ni(II) | 0.61 | 0.49 | 0.48 |
| $Fe_{total}$ | 0.01 | 0.12 | 0.52 |
| Zn(II) | 0.21 | 0.06 | 0.01 |
| Cu(II) | 0.07 | 0.01 | 0.01 |
| pH | 6.5 | 6.6 | 8.2 |